Wang et al. *Zool. Res.* 2023, 44(1): 126−141
https://doi.org/10.24272/j.issn.2095-8137.2022.397

ZR | Zoological Research

Article Open Access

Dusp1 regulates thermal tolerance limits in zebrafish by maintaining mitochondrial integrity

Ying Wang[1,2,3], Hua-Min Wang[1,2,3], Yan Zhou[1,2,3], Ling-Hong Hu[1,2,3], Jing-Ming Wan[1,2,3], Ji-Hui Yang[1,2,3], Hong-Bo Niu[1,2,3], Xiu-Ping Hong[1,2,3], Peng Hu[1,2,3], Liang-Biao Chen[1,2,3,*]

[1] *International Research Center for Marine Biosciences*, *Ministry of Science and Technology*, *Shanghai Ocean University*, *Shanghai* 200120, *China*

[2] *Key Laboratory of Exploration and Utilization of Aquatic Genetic Resources*, *Ministry of Education*, *Shanghai Ocean University*, *Shanghai* 200120, *China*

[3] *Shanghai Collaborative Innovation for Aquatic Animal Genetics and Breeding*, *Shanghai Ocean University*, *Shanghai* 200120, *China*

ABSTRACT

Temperature tolerance restricts the distribution of a species. However, the molecular and cellular mechanisms that set the thermal tolerance limits of an organism are poorly understood. Here, we report on the function of dual-specificity phosphatase 1 (DUSP1) in thermal tolerance regulation. Notably, we found that *dusp1*$^{-/-}$ zebrafish grew normally but survived within a narrowed temperature range. The higher susceptibility of these mutant fish to both cold and heat challenges was attributed to accelerated cell death caused by aggravated mitochondrial dysfunction and over-production of reactive oxygen species in the gills. The DUSP1-MAPK-DRP1 axis was identified as a key pathway regulating these processes in both fish and human cells. These observations suggest that DUSP1 may play a role in maintaining mitochondrial integrity and redox homeostasis. We therefore propose that maintenance of cellular redox homeostasis may be a key mechanism for coping with cellular thermal stress and that the interplay between signaling pathways regulating redox homeostasis in the most thermosensitive tissue (i.e., gills) may play an important role in setting the thermal tolerance limit of zebrafish.

Keywords: Redox homeostasis; Zebrafish; Ectothermal; Mitochondrial fission; Thermal stress; MAPK

INTRODUCTION

Temperature shifts affect numerous biological processes in all species. For ectotherms, temperature is a primary determinant of species range limits (Hellmann et al., 2008). In recent years, aquatic biodiversity and ecosystem functions have been severely threatened by global climate change (Halpern et al., 2008; Vitousek et al., 1997), with many tropical species already living near their upper lethal thermal limits (Somero, 2010, 2011; Stillman, 2003) and many polar species lacking the ability to tolerate rising water temperatures (Peck et al., 2014). Revealing the mechanisms that determine the thermal tolerance limits of organisms is important for the conservation of biodiversity and improvement of thermal tolerance in agricultural species.

Various studies have explored the mechanisms of thermal limitations in ectothermal animals (MacMillan, 2019), leading

Received: 26 October 2022; Accepted: 23 November 2022; Online: 23 November 2022

Foundation items: This work was supported by the National Key Research and Development Program of China (2018YFD0900601) and National Natural Science Foundation of China (32130109)

*Corresponding author, E-mail: lbchen@shou.edu.cn

to proposing of two main models. The oxygen and capacity limitation of thermal tolerance (OCLTT) model suggests that animal performance is set by the effects of temperature on oxygen supply and demand (Pörtner et al., 2017; Pörtner, 2012). The ionoregulatory collapse model proposes that animals experience local and systemic disruptions in ion and water balance, which drive chilling injury and chill coma (Overgaard & MacMillan, 2017). However, in both models, the underpinning molecular and cellular mechanisms remain to be fully elucidated.

As ectotherms and the most speciose group of vertebrates, the mechanisms underlying thermal responses in fish have been extensively studied. In response to external temperature changes, fish can gradually establish adaptive phenotypes via a wide range of biochemical, metabolic, and physiological modifications. Studies have shown that temperature adaptation can be achieved through the production of temperature-specific isoenzymes (Somero & Hochachka, 1971), reformation of membrane lipids and unsaturated fatty acids (Johnston & Roots, 1964), recruitment of various muscle fibers (Gerlach et al., 1990), synthesis of molecular chaperones (Dilorio et al., 1996; Fader et al., 1994), and modification of mitochondrial density and characteristics (Pichaud et al., 2017; St-Pierre et al., 1998). Recent advances in comparative transcriptomics and genomics have allowed the exploration of genome-wide transcriptional responses elicited by temperature stress in fish (Gracey et al., 2004; Hu et al., 2015; Ju et al., 2002; Logan & Somero, 2011). These studies have revealed various temperature-responsive genes involved in different biological processes, such as metabolism and apoptosis regulation, many of which are involved in cell death or survival under conditions of environmental stress.

By comparing the levels of cellular damage in various organs under lethal low and high temperatures, we found that the gill is the most sensitive organ to thermal stress, followed by the kidney (Hu et al., 2016, 2021). The degree of cellular apoptosis or necrosis in fish gills is negatively correlated with cold stress resistance (Hu et al., 2016). As gills are the primary organ for oxygen intake and ion regulation, these observations accord with both the OCLTT and ionoregulatory collapse models of thermal limits in fish, suggesting that molecular mechanisms regulating cell death and survival play important roles in determining the lower and upper thermal limits of ectotherms.

Activation of the MAPK signaling pathway is closely related to environmental stress (Kültz & Burg, 1998). The MAPK signaling pathway is widely conserved across species and determines cell fate through the integration of various signals (Rauch et al., 2016; Winter-Vann & Johnson, 2007). As part of the MAPK signaling network, mitogen-activated protein kinase phosphatase-1 (MKP-1), also known as dual-specificity phosphatase 1 (Dusp1), plays a critical role in regulating MAPK signaling (Cai et al., 2019; Niu et al., 2017; Tomalty et al., 2015). DUSP1 specifically dephosphorylates ERK1/2, JNK, and P38 on tyrosine and serine/threonine residues, resulting in the inactivation of the three major MAPK family members (Lang & Raffi, 2019). *Dusp1* is considered an immediate early response gene and can be induced by multiple stimuli, including growth factors (Comalada et al., 2012; Wancket et al., 2012), cellular stress (Li et al., 2011; Sha et al., 2019), and retinoids (Zhuang et al., 2021). In a previous study, we found that *Dusp1* is differentially expressed in the tissues of fish with disparate cold survival temperatures, suggesting a role in regulating cold tolerance limits (Hu et al., 2016).

In the current study, we generated *Dusp1* knockout genotypes in zebrafish and investigated the role of DUSP1 in regulating temperature tolerance limits. We further elucidated the DUSP1 signaling cascades involved in this process.

MATERIALS AND METHODS

Ethics approval

All applicable international, national, and/or institutional guidelines for the care and use of animals were strictly followed. All animal sample collection protocols complied with the current laws of China. All animal procedures performed in this research were reviewed and approved by the Institutional Animal Care and Use Committee of the Shanghai Ocean University (SHOU), Shanghai, China (approval No. 20171021).

Construction of *dusp1* knockout zebrafish

Wild-type (WT) AB strain zebrafish (*Danio rerio*) were acquired from the National Zebrafish Center (Wuhan, China). These zebrafish were used as parents to generate *dusp1*$^{-/-}$ mutant fish. A single site (5'-GGAAGTGCCCACTATCGATT-3') within exon 1 of the zebrafish *dusp1* gene was selected as the target site for the CRISPR-Cas9 system using the ZiFiT Targeter (http://zifit.partners.org/ZiFiT) online tool. Guide RNA (gRNA) was synthesized and purified using a MAXIscript T7 Kit (Ambion, USA) following the manufacturer's protocols. To prepare Cas9 mRNA, 1 μg of pT7-2NLS-Cas9 plasmid (provided by Peking University Zhang Bo Lab) was linearized by Xbal (NEB, USA) and purified using a DNA Clean & Concentrator-5 Kit (Zymo Research, USA). The linearized plasmid DNA was used as a template to synthesize capped Cas9 mRNA with the mMESSAGE mMACHINE T7 ULTRA Kit (Thermo, USA). The product was purified using a RNeasy Mini Kit (Qiagen, Germany).

Fertilized zebrafish embryos at the one-cell stage were collected and placed on an agar plate for microinjection. Single guide RNA (sgRNA) and Cas9 mRNA solutions were diluted with the injection buffer (sgRNA: 100 ng/μL, Cas9 mRNA: 400 ng/μL). This mixture (1 nL) was injected into the zebrafish embryos. The injected embryos were incubated in E3 medium at 28.5 ℃ until hatching.

Genomic DNA from the tail of one-month-old CRISPR-cas9-treated fish was extracted using the NaOH/Tris-HCl method (Zhang et al., 2012). The genomic DNA was subjected to polymerase chain reaction (PCR) amplification using primers: dusp1-F (5'-TTTGGTTGGCCAGGCTCAA-3') and dusp1-R (5'-AAACGACACTCTGGTATTCC-3'), followed by T7E1 assay (Kim et al., 2009). Individuals with the desired DNA banding pattern from the T7E1 assay were retained and the PCR products were Sanger sequenced to verify the genetic mutation. Three individuals were identified as *dusp1* mutation founders (F0) with different mutations in the *dusp1* gene. The

individual with the mutation shown in Figure 1B and Supplementary Figure S1 was used to breed offspring for this study.

Obtaining *dusp1*$^{-/-}$ homozygous mutants

The F1 males and females derived from the chosen F0 founder were crossed to produce F2 offspring. To screen for *dusp1* homozygous mutants, tail tissue from three-week-old fish was obtained for DNA preparation. The *dusp1*$^{-/-}$ homozygotes were screened using target site-specific primers and PCR-based sequencing (Supplementary Figure S1). We used the crosses of dusp1$^{+/-}$ sibling pairs to produce sufficient fish. Different dusp1 genotypes (i.e., *dusp1*$^{-/-}$, *dusp1*$^{+/-}$, and WT) of the same age and genetic background were thus used for the temperature challenge experiments.

Fish preparation and thermal challenge design

All fish (WT or *dusp1* mutants) were bred at 28 °C±1 °C under a 10 h/14 h light/dark cycle and fed with hatched artemia. Fish used for each temperature treatment were bred from the same batch and from the same parents. To set up the temperature experiments, six-month-old age and weight-matched zebrafish were randomly divided into at least three groups (i.e., biological replicates). Each group consisted of at least 10 fish. The animals were maintained in well-oxygenated water tanks of the same size (60 cm×40 cm×40 cm) at 28 °C for a week with regular feeding, and were food deprived overnight prior to the experiment.

Thermal tolerance tests were performed in a temperature-adjustable incubator with pre-designed stepwise cooling and heating schemes. For cooling, the water temperature was set to decline from 28 °C to 18 °C at a rate of 0.85 °C/h, with the tank then maintained at 18 °C for 12 h. After that, the water temperature declined to 8 °C within 12 h, with the tank then maintained at this temperature. For warming, the water temperature was set to increase linearly from 28 °C to 38 °C at a rate of 0.85 °C/h, with the tank then maintained at that temperature for 4 h. All control groups were maintained at the regular 28 °C conditions (Figure 1A).

Impact of *dusp1*-deficiency on thermal tolerance

To test the function of *dusp1* in thermal tolerance, adult *dusp1*$^{-/-}$ zebrafish together with their WT and/or heterozygous siblings of similar size and weight were subjected to the temperature challenges stated above. In each experiment, for each genotype, a total of 30 fish were randomly assigned to three same-sized glass tanks (n=10 fish per tank). Time and temperature at which a fish experienced loss of equilibrium (LOE) under the given thermal challenge were recorded. We carried out at least three repeats for each cold and heat tolerance assay with siblings produced from different batches of *dusp1*$^{+/-}$ fish crosses.

Identification of thermal sensitive tissues through apoptosis detection

For tissue dissection, fish were anaesthetized with an overdose of MS-222 and killed immediately by decapitation. Six tissues (i.e., gill, brain, liver, muscle, heart, and kidney) were dissected from *dusp1*$^{-/-}$ and WT fish at three determined temperature-time points: i.e., 8 °C (12 h), 38 °C (4 h), or normal temperature (28 °C) during the thermal challenge experiments. The tissues were immediately fixed in 4% paraformaldehyde solution (Servicebio, China) at 4 °C overnight for paraffin sectioning. Paraffin blocks were sectioned at 6 μm thickness using a microtome, after which the tissue sections were deparaffinized using xylene. The sections were treated with sodium citrate buffer (pH 6.5) at 95 °C for 5 min, followed by TUNEL staining using a TUNEL FITC Apoptosis Detection Kit (Vazyme, China) following the manufacturer's instructions. The sections were then counterstained with 4',6-diamidino-2-phenylindole (DAPI, 500 ng/mL) for 5 min and photographs were immediately taken with a laser confocal microscope (Zeiss, Germany).

RNA sequencing (RNA-seq) and data analysis

Gills of the WT and *dusp1*$^{-/-}$ zebrafish were dissected at three

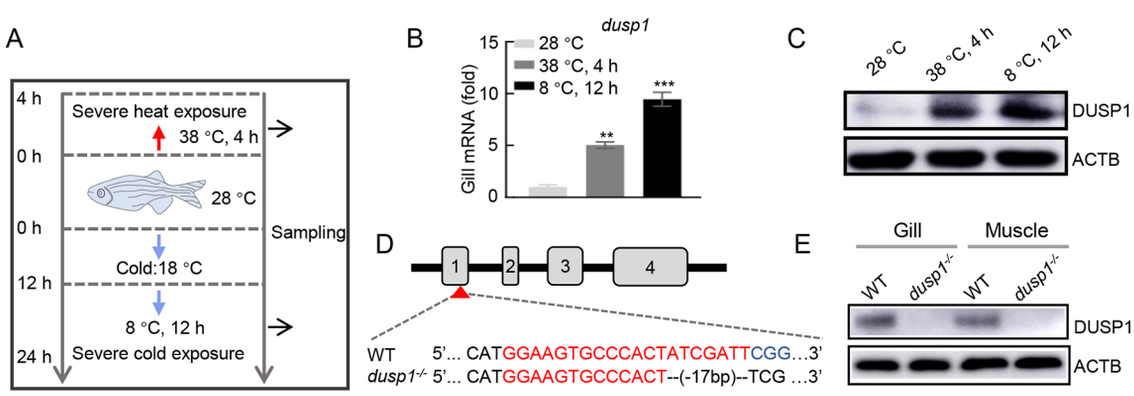

Figure 1 Temperature-induced expression of *dusp1* and deletion of *dusp1* in zebrafish

A: Flowchart depicting cold and hot temperature treatments in zebrafish for sampling. Three-month-old zebrafish reared at 28 °C were subjected to cold treatment by exposure to 18 °C for 12 h and 8 °C for 12 h. Hot temperature treatment was carried out by exposing fish to 38 °C for 4 h, with controls maintained at 28 °C. Samples for qRT-PCR and immunoblot analysis were collected at three temperature-time points (28 °C, 38 °C 4 h, 8 °C 12 h). Sample size: n=30. B: Dusp1 expression under cold and hot treatment measured using qRT-PCR compared with normal temperature controls. Data are mean±*SD*. **: P<0.01; ***: P<0.001. C: Western blot analysis of DUSP1 protein levels in gills under thermal stress, with ACTB as the loading control. D: Schematic of targeted dusp1 gene editing by CRISPR/Cas9 and disruption of dusp1 at exon 1. E: Western blot validation of loss of dusp1 in dusp1-KO fish indicated by two tissues examined.

time-temperature points (i.e., 28 °C, 18 °C (12 h), or 38 °C (4 h)) in the thermal challenge experiments. To ensure consistency between samples, WT and *dusp1*$^{-/-}$ zebrafish individuals were sampled in parallel at the determined time points. At each temperature/time point, samples from the three biological replicates were collected. In total, 18 samples (two genotypes×three time points×three biological replicates) were sequenced individually.

Total RNA in gill tissue (500 mg) from each sample was extracted using TRIzol Reagent according to the manufacturer's protocols (Invitrogen, USA). Bioanalyzer Chip RNA 7500 Series II (Agilent, USA) was used to assess RNA quality. A Qubit fluorometer (Thermo, USA) was used to determine total RNA concentration. PolyA+ mRNA was purified from 2 μg of total RNA for each sample and used to construct an RNA-seq library for high-throughput Illumina sequencing.

Clean reads were mapped to the reference zebrafish genome (version GRCz11) using HISAT v2.0.4 with default values (Kim et al., 2015). Cufflinks v2.2.1 (Trapnell et al., 2010) was used to normalize gene expression to the quantified transcription level (FPKM; fragments per kilobases per million). Differentially expressed genes (DEGs) were calculated using the R package edgeR (Robinson et al., 2010). Fisher's exact test was then used to identify DEGs (fold-change≥2 ($\log_2$FC≥1) and false discovery rate (FDR)<0.05). Functional enrichment was performed using the web server WebGestalt (Wang et al., 2017) referencing the Kyoto Encyclopedia of Genes and Genomes (KEGG) pathway database (Kanehisa et al., 2010).

Dusp1 overexpression in *dusp1*$^{-/-}$ zebrafish embryos

His-tagged dusp1 mRNA (*Dusp1-HIS*) was subcloned into the pCS2+ vector for *in vitro* transcription. The tagging of mRNA with His-tag was performed to facilitate estimation of expression efficiency of the injected mRNA. Capped sense RNA was synthesized using a mMESSAGE mMACHINE SP6 Transcription Kit (Thermo, USA) *in vitro*. In total, 1 nL of 200 ng/μL *dusp1* or *gfp* mRNA was injected into the *dusp1*$^{-/-}$ embryos at the one-cell-stage. Embryos held under normal cultivation temperature (28 °C) for 12 h were then cooled (to 12 °C) or heated (to 34 °C) at a rate of 0.85 °C/h. The survival rate was determined after 6 h by counting the percentage of dead embryos.

Reactive oxygen species (ROS) detection in fish gills

To measure ROS production in fish gills, fresh gills were dissected from WT and *dusp1*$^{-/-}$ fish at the determined temperature-time points during the thermal challenge experiments. The gills were separated into single branchial filament pieces under a microscope, washed with phosphate-buffered saline (PBS) three times, then incubated with the redox-sensitive probe DCFH-DA (Beyotime, China, 1:1 000 in PBS). After incubation in the dark for 15 min at room temperature, the ROS-detection solution was immediately removed, and the gill filaments were washed three times with PBS. Fluorescence microscopy images were taken on an inverted fluorescence microscope (Zeiss, Germany). Fluorescence intensity was quantitated using ImageJ software.

Measurement of adenosine triphosphate (ATP) level in fish gills

Cellular ATP was measured using an ATP Assay Kit (Beyotime, China) according to the instructions provided by the manufacturer. In brief, fish gill tissues were first lysed using lysis buffer, then centrifuged at 12 000 r/min for 5 min at 4 °C, with the supernatant collected for further assessment. The protein concentration in the supernatant was analyzed using a BCA Kit (Beyotime Biotechnology, China). The supernatant was pipetted into a 96-well plate (100 μL/well) followed by ATP detection working solution (100 μL/well). The plate was then placed at room temperature for 5 min. The relative light unit (RLU) was determined using a chemiluminometer. The ATP concentration was determined by referring to the RLU standard curve generated using the standards provided in the kit. Finally, the ATP level was calculated using the following equation: ATP level=ATP concentration/total protein concentration.

Mitochondrial staining of gill sections

Fresh gill tissues collected from the experimental and control animals were immediately submerged in fixing solution (10 mL of formaldehyde, 1 g of calcium chloride, and 90 mL of double-distilled water) overnight for fixation. The tissue was then embedded in paraffin, sectioned into 4 μmol/L slices, dried, dewaxed, and washed with water. The sections were then treated with Biebrich Scarlet-Acid Fuchsin (Sigma, USA) for 17 h. After that, the slides were washed with water and placed in 70%, 80%, and 95% alcohol for 30 s sequentially for dehydration. The sections were subsequently stained with 0.1% Fast-Green (Sigma, USA) in 1×PBS for 20 s. After twice washing with water, the sections were immersed for 5 min in each of the following: 100% alcohol, 100% alcohol, alcohol: xylene (1:1). After complete air-drying, the slides were observed and photographed under a light microscope. Quantification of mitochondrial number was performed using ImageJ software.

Transmission electron microscopy (TEM) examination of mitochondrial structure

Fresh gills excised from fish or HEK293T cells scrapped from the culture plate were transferred to an Eppendorf tube containing fresh TEM fixative (Servicebio, China) for fixation overnight at 4 °C. The fixed tissues were washed three times (15 min each) with 1×PBS (pH 7.4). The samples were post-fixed with osmium tetroxide solution (Sigma, USA), dehydrated in serial ethanol dilutions (Sigma, USA), and embedded in epoxy resin. The resin-embedded samples were moved to a 65 °C oven for polymerization for more than 48 h. The resin blocks were then removed from the embedding models, cooled at room temperature, cut to 60–80 nm thick slices using an ultra-microtome, and fished out onto 150 mesh cuprum grids with formvar film. The tissues were then stained with uranyl acetate and lead citrate (Electron Microscopy Sciences, USA). Imaging was performed with a HT7800 TEM (Hitachi, Japan).

Oxygen consumption assessment

Oxygen consumption was determined using a Respiratory

Movement Measuring Instrument (Jingyu, China) according to the provided instructions. Briefly, adult WT and *dusp1*$^{-/-}$ zebrafish of similar size, weight, and age were selected as experimental specimens. Three females and three males were selected for each genotype for each temperature treatment. Measurement was run on one fish at a time. A single fish was placed into a water chamber, after which the remaining air was evacuated with running water and the chamber was closed tight. The chamber temperature (28 °C, 8 °C, and 38 °C) was maintained by the water inside and surrounding the chamber. For cold challenge, 8 °C cold water was used, while for heating, a thermostatic heating rod was used to control the water temperature. Oxygen consumption rates were monitored in real time. When the chamber O_2 reached 0.4 mg/L, the oxygen consumption rate curve became steady, and that point was set as the starting point to compare fish. Oxygen consumption was monitored for 25 min. Oxygen consumption of the six fish for each genotype in each temperature treatment was averaged to deduce the O_2 consumption rate of the genotype at that temperature. As we weighed fish prior to the experiment and only fish with similar weight (0.72±0.11 g) and body length (3.67±0.3 cm) were used, O_2 consumption rates were not normalized by mass.

Construction of DUSP1 knockout HEK293T cell line

The human HEK293T cell line (American Type Culture Collection, ATCC, USA) was cultured in high-glucose Dulbecco's modified Eagle's medium (DMEM) supplemented with 10% fetal calf serum (FCS) and 1% penicillin/streptomycin in 5% CO_2 at 37 °C. All experiments were conducted when the culture plates achieved around 80% confluency. The cell line was tested to be free of *Mycoplasma* contamination.

To create a dusp1 knockout cell line, two sgRNAs targeting exon 1 and exon 2 of the human *dusp1* gene were designed, synthesized, and cloned into PX458 plasmids (Addgene, USA), then transfected into the HEK293T cells with Lipofectamine (Thermo, USA). After screening for enhanced green fluorescent protein (EGFP) expression, monoclonal cells were established by serial dilution and culture, and those monoclonal cells with correct dusp1 knockout were identified by sequencing. The knockout efficiency of the cell lines was checked by western blot analysis. Cell lines in which the first and second exons of dusp1 were removed were chosen for further experiments.

Physiological measurements of *dusp1*$^{-/-}$ HEK293T cells

To measure the ROS level in HEK293T cells, the cells of each genotype (*dusp1*$^{-/-}$ and WT) were divided into three dishes and grown for one day at 37 °C. Two dishes of the same genotype were transferred to 43 °C and 13 °C, respectively (approximately the upper and lower lethal temperatures of the cells determined in this work), with one remaining at 37 °C. After 5 h at 43 °C or 15 h at 13 °C, dihydroethidium (DHE, Solarbio, China) was added to the cell cultures (including the 37 °C cultured cells as the control) to a final concentration of 10 μm. The cells were incubated at the treated temperatures for 30 min. The staining solution was removed, after which the cells were suspended in 0.25% trypsin solution, collected, washed with serum-free cell culture medium three times, and suspended in 1×PBS. ROS activity was measured using fluorescence flow cytometry (BD Biosciences, USA). Data were analyzed using FlowJo software.

To measure mitochondrial membrane potential, *DUSP1*$^{-/-}$ and WT HEK293T cells were cultured, and measurements were performed using membrane-permeant JC-1 dye. Solutions from the JC-1 Kit (Beyotime, China) were added, followed by incubation for 20 min at three temperatures (continued at 37 °C, 43 °C for 5 h, or 13 °C for 15 h) in 12-well plates. The supernatant was removed, and the staining buffer provided by the kit was used to wash the cell twice. Cell culture medium with serum (1 mL) was added and the cells were then photographed under a fluorescence microscope. The fluorescence intensity of the sample was determined by ImageJ and the red/green ratio was calculated to infer mitochondrial membrane potential.

To measure ATP production, *DUSP1*$^{-/-}$ and WT HEK293T cells were cultured and treated under the same thermal stress conditions as above. The culture medium was removed, and cells were lysed using the lysis buffer provided by the ATP Assay Kit (Beyotime, China). The ATP level was measured following the same procedures used to measure ATP in the fish gill.

MitoTracker staining

MitoTracker Red CMXRos (Beyotime, China) was used to label mitochondria in the HEK293T cells. Cells (WT and *DUSP1*$^{-/-}$) were cultured to 80% confluency at 37 °C and exposed to three temperatures (continued at 37 °C, 43 °C for 5 h, or 13 °C for 15 h) in 12-well plates. After removing the medium, 500 μL of working solution of MitoTracker Red CMXRos (Beyotime, China) at 200 nmol/L was added to each well, followed by incubation at 37 °C for 30 min. The working solution was then removed and fresh cell culture medium pre-warmed to 37 °C was added. The cells were visualized and photographed under a Zeiss fluorescence microscope. ImageJ was used to measure fluorescence intensity.

Propidium iodide staining

Propidium iodide (PI, Sigma, USA) staining was used to measure the rate of cell death in HEK293T cells exposed to lethal temperatures. Briefly, cells were treated with PI and incubated under different treatment conditions in a 5% CO_2 incubator for 15 min in the dark. Hoechst (Beyotime, China) was added to the culture medium as a nucleus marker. PI-positive cells were determined using an inverted fluorescence microscope. Quantitative analysis of fluorescence intensity was performed using ImageJ software.

Cell viability assay

HEK293T cells (*DUSP1*$^{-/-}$ and WT) were seeded in a 96-well plate at a density of 8×10^3 cells/well and incubated in 18 °C or 40 °C incubators for 6 h. The CCK-8 assay (Beyotime, China) was used to measure cell viability in a time series at intervals of 0, 24, 48, or 72 h after an initial 6 h of culture following the manufacturer's manual. Briefly, to measure cell viability, 10 μL of CCK-8 solution and 100 μL of medium were added to each well. Absorbance of each well was recorded at 450 nm using a

BioTek microplate reader (Thermo, USA). All experiments were repeated at least three times, with triplicates for each sample. Cell viability was calculated as $((OD_{treated}-OD_{blank})/(OD_{control}-OD_{blank})\times100\%)$.

Quantitative real-time PCR

Total RNA extraction and quantification were performed as above. For each sample, 1 μg of total RNA was used to generate cDNA using an RT-PCR Kit (Takara, Japan). Quantitative real-time PCR (qRT-PCR) was performed using a FastStart Universal SYBR Green Master Kit (Roche, Germany) according to the manufacturer's instructions and results were analyzed using the LightCycler 480 system (Roche, Germany) with the two-step method. We used *β-actin* as a reference gene and quantified the expression of target genes using the $2^{-\Delta\Delta CT}$ method (Pfaffl, 2001). Primer sequences used in this study include 5' CTCTGTATG ATCAGGGTGGCCC 3' and 5' CGGTGATCCCCAACATGTCC 3' for *dusp1*; and 5' TGTCCCTGTATGCCTCTGGT 3' and 5' AAGTCCAGACGGAGGATG 3' for *β-actin*. The PCR conditions are as follows: 10 min at 95 °C for DNA denaturation, followed by target cDNA amplification (40 cycles at 95 °C for 10 s and 30 s at 60 °C).

Western blot analysis

The gill and HEK293T cell samples were homogenized and lysed in RIPA buffer (Sigma, USA) containing phenylmethylsulfonyl fluoride (PMSF) (Thermo, USA) and centrifuged at 10 000 ×*g* for 10 min at 4 °C. The supernatant was removed and stored at −80 °C for future use. Quantification of total protein was conducted using a BCA Protein Assay Kit (Thermo, USA). Samples were denatured in boiling water for 10 min in sample buffer (Takara, Japan). A total of 30 μg of protein from each sample was separated using 15% sodium dodecyl-sulfate polyacrylamide gel electrophoresis (SDS-PAGE). The resolved proteins were transferred to a polyvinylidene difluoride (PVDF) membrane, which was then blocked with 5% milk or bovine serum albumin (BSA) in Tris-buffered saline with 0.1% Tween-20. Primary antibodies, including anti-DUSP1 (1:1 000; Abcam, UK), anti-phospho-pERK (1:2 000; CST, USA), anti-phospho-p38 (1:2 000; CST, USA), anti-p53 (1:5 000, Huaan, China), anti-phospho-DRP1S616 (1:2 000; CST, USA), anti-BAX (1:500, Huaan, China), anti-cleaved CASPASE-3 (1:2 000; Huaan, China), and anti-ACTIN (1: 10 000; Abcam, UK), and secondary antibodies, including goat anti-mouse (1:10 000, Huaan, China) and goat anti-rabbit (1:10 000, Huaan, China), were used to detect the corresponding proteins. Target proteins were visualized using an ECL detection system (Bio-Rad, USA).

Statistical analysis

All values are presented as mean±standard deviation (*SD*). The values $P<0.05$ (*), $P<0.01$ (**), and $P<0.001$ (***) exhibited significance in one-way analysis of variance (ANOVA) and Student's *t*-test. The Kaplan-Meier test was used to estimate significant differences in survival rate. Statistical analyses were carried out using GraphPad (GraphPad Prism v5). $P\leq 0.05$ was considered statistically significant.

RESULTS

Temperature stress up-regulated *dusp1* expression in zebrafish

To evaluate the role of *dusp1* in regulating temperature tolerance limits in fish, we first examined gene expression in the temperature-sensitive gills in response to temperature stress. We quantified *dusp1* mRNA levels under low and high lethal temperature challenge following the protocols shown in Figure 1A. Compared to control fish reared under normal temperature (28 °C), fish challenged by cold (8 °C) and heat (38 °C) stress showed substantial up-regulation of *dusp1* mRNA (Figure 1B) and protein expression levels (Figure 1C).

Generation of *Dusp1* mutant zebrafish

We used the CRISPR/Cas9 system to mutate the *dusp1* gene in zebrafish. We successfully introduced a 17 bp deletion in the first exon of *dusp1* (Figure 1D; Supplementary Figure S1A). The corresponding transcript resulted in a prematurely terminated 39 amino acid polypeptide, which differed from the WT 360 amino acid protein (Supplementary Figure S1B). The absence of DUSP1 in the mutant fish was verified by western blot analysis of proteins extracted from the gills and muscle (Figure 1E). No significant differences in morphology, body weight (0.38±0.05 g), or body length (3.5±0.1 cm) were observed between the *dusp1* KO (F2 generation) and WT zebrafish (Supplementary Figure S1C).

Elevated apoptosis and lower tolerance to temperature stress in *dusp1* mutants

The mutant fish were challenged at 8 °C to examine cold resistance. The survival rate differed significantly among the *dusp1*$^{-/-}$, *dusp1*$^{+/-}$, and WT fish, with survival time reduced by 50% and 25% in the homozygous and heterozygous fish, respectively, compared with the WT fish (Figure 2A). The lower cold tolerance of the mutant fish was correlated with accelerated cell apoptosis in the gills. Under 8 °C treatment, a significantly greater proportion of cells undergoing apoptosis occurred in the gills of the *dusp1*$^{-/-}$ fish compared to the WT fish (Figure 2B). However, no significant difference in apoptotic signals was found between the *dusp1*$^{-/-}$ and WT fish at 28 °C (Figure 2B). Cell apoptosis severity in the gills was negatively correlated with cold tolerance capability. After prolonged cold treatment at 8 °C for 12 h, apoptosis occurred in 58% of the cells in the gills of the *dusp1*$^{-/-}$ mutants, much higher than that of the WT fish (30%) (Figure 2B, C). No significant apoptotic signals were detected in tissues other than the gills (Supplementary Figure S2A).

To investigate the performance of *dusp1* knockout fish under high temperature stress, we measured survival time at 38 °C. Neither *dusp1*$^{-/-}$ nor *dusp1*$^{+/-}$ fish survived beyond 6 h at this temperature, whereas at least 50% of WT siblings survived and were viable for a prolonged period (Figure 2D). Interestingly, under high temperature challenge, apoptotic signals were also only abundantly detected in the gills (Figure 2E), with sporadic signals visible in a few other tissues (Supplementary Figure S2B). Furthermore, the rate of apoptosis in the *dusp1*$^{-/-}$ fish gills outpaced that of the WT fish (Figure 2F), similar to the cold lethal temperature results.

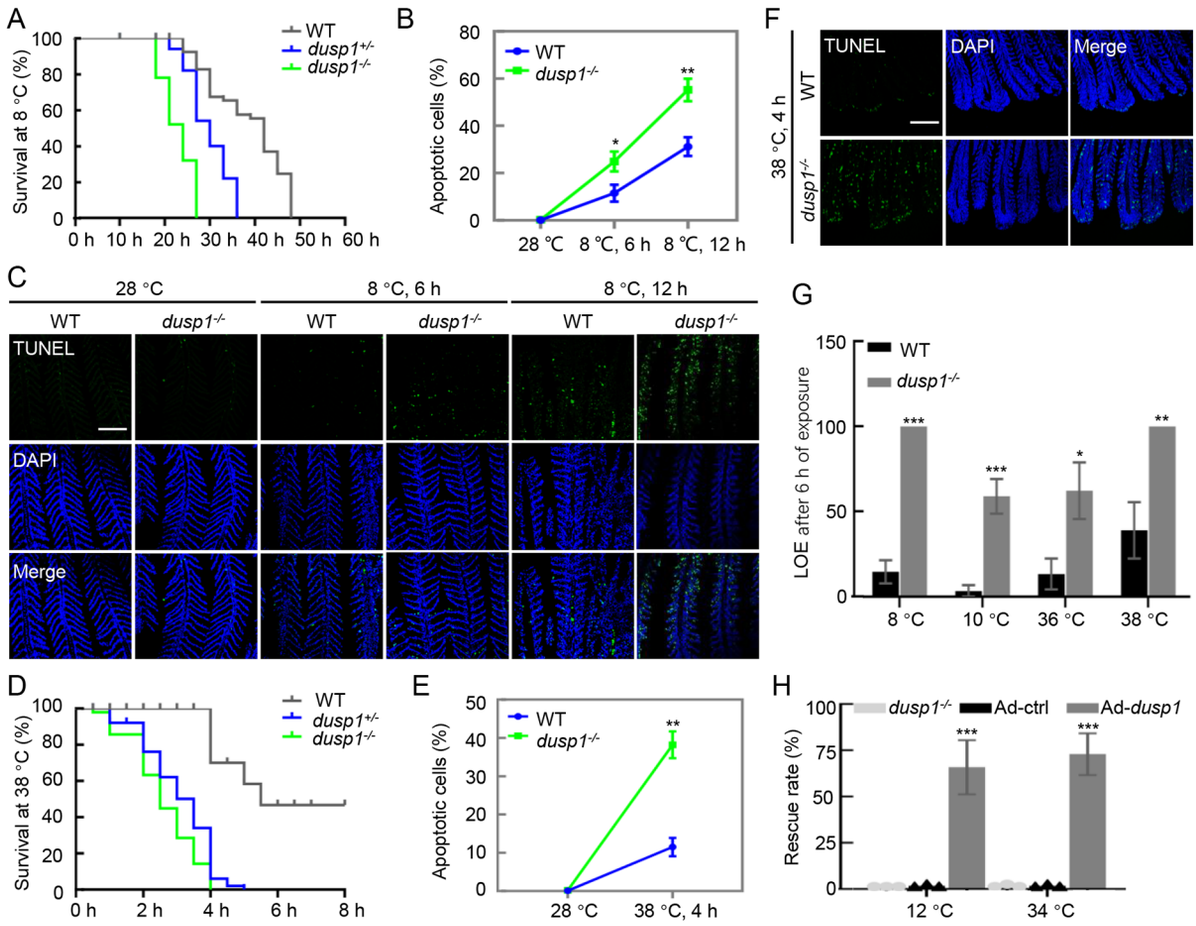

Figure 2 Negative impacts of dusp1 deletion on thermal stress tolerance in mutant fish

Thermal challenges were the same as described above. Sample size was 30 for each thermal challenge and at least three biological replicates were performed. A: Kaplan-Meier curves of three genotypes (*dusp1*$^{-/-}$, *dusp1*$^{+/-}$, and WT) treated by 8 °C exposure. B: Quantified apoptotic signal in gills under cold exposure analyzed by ImageJ software. Student's *t*-test, *: $P<0.05$; **: $P<0.01$. C: TUNEL assay showing apoptotic signal in gills under 8 °C treatment. Scale bar: 100 μm. D: Kaplan-Meier curves of three genotypes (*dusp1*$^{-/-}$, *dusp1*$^{+/-}$, and WT) under 38 °C exposure. E: Quantified apoptotic signal in gills under hot exposure analyzed by ImageJ software. Student's *t*-test, **: $P<0.01$. F: TUNEL assay of apoptosis in gills under hot (38 °C for 4 h) treatment. Scale bar: 100 μm. G: Differences in upper and lower lethal temperature tolerance between WT and *dusp1*$^{-/-}$ zebrafish. LOE indicates loss of equilibrium. Half survival rates (i.e., LOE rate) of *dusp1*$^{-/-}$ fish occurred at 10 °C and 36 °C, respectively, under cold and heat challenges, while WT fish exhibited half survival rates at 8 °C and 38 °C, respectively. One-way ANOVA, *: $P<0.05$; **: $P<0.01$; ***: $P<0.001$. H: Rescue of *dusp1*$^{-/-}$ mutant by zebrafish dusp1 mRNA (Ad-*dusp1*). Adding dusp1 mRNA restored the survival rate of embryos under cold (8 °C) and hot (38 °C) treatment. The same amount of GFP mRNA (Ad-ctrl) and *dusp1*$^{-/-}$ embryos without injection were used as controls. One-way ANOVA, ***: $P<0.001$.

These observations suggest that *dusp1* serves as an important regulator of thermal tolerance in zebrafish by inhibiting apoptosis in sensitive cells. Thermal tolerance measurements showed that the LOE rates were higher in *dusp1*$^{-/-}$ fish than in WT fish at the different extreme temperatures (Figure 2G).

To further validate the protective role of *dusp1* under adverse temperatures, we performed rescue experiments by microinjecting *dusp1* or *gfp* mRNA into *dusp1*$^{-/-}$ embryos. In total, 65% (312 out of 480) and 68% (368 out of 542) of embryos survived 6 h of exposure to cold (12 °C) and hot (34 °C) temperatures, respectively (Figure 2H), whereas no embryos survived in the *dusp1*$^{-/-}$ group without *dusp1* mRNA or with *gfp* mRNA injection, confirming the positive function of *dusp1* in thermal tolerance.

Comparison of gene expression profiles between *dusp1*$^{-/-}$ and WT zebrafish based on RNA-seq analysis

We performed RNA-seq analysis of gill samples from WT and *dusp1*$^{-/-}$ zebrafish under normal (28 °C), high (38 °C for 4 h), and low (8 °C for 12 h) temperatures. Comparing quantified gene expression levels between WT and *dusp1*$^{-/-}$ zebrafish, we identified thousands of DEGs at each temperature treatment, with the smallest number of DEGs identified in the normal temperature group (Supplementary Figure S3). KEGG functional annotation of the DEGs revealed seven pathways, including the NOD-like receptor signaling pathway and Toll-like receptor signaling pathway, enriched at 28 °C. The RIG-I-

like receptor signaling pathway, ribosome biogenesis in eukaryotes, oxidative phosphorylation pathway, and FoxO signaling pathway were enriched at 38 °C, while the Toll-like receptor signaling pathway, cytosolic DNA-sensing pathway, and p53 signaling pathway were enriched at 8 °C (Figure 3A). Other pathways were common to at least two treatment-time points. The enrichment of KEGG pathways clearly indicated that loss of *dusp1* affected multiple biological processes. Notably, the oxidative phosphorylation pathway was significantly enriched at all three treatment-time points, and nine genes associated with this pathway were significantly down-regulated (Figure 3B), suggesting impairment of oxidative phosphorylation in mutant mitochondria.

Dusp1 deficiency promoted ROS production and apoptosis in the gill

The marked differences between *dusp1*$^{-/-}$ and WT zebrafish in the expression of genes associated with oxidative phosphorylation are suggestive of redox dysregulation in the *dusp1*$^{-/-}$ fish. Thus, we measured ROS levels in the gill tissues of both types of fish. The *dusp1*$^{-/-}$ fish showed similar ROS levels as the WT fish under normal conditions but showed two-fold higher levels of ROS when exposed to cold (8 °C/12 h) and hot (38 °C/4 h) temperatures (Figure 3C, D). Correspondingly, compared to WT fish, protein quantification revealed a 2-fold up-regulation in apoptosis-associated factor caspase-3 under low and high temperature challenge

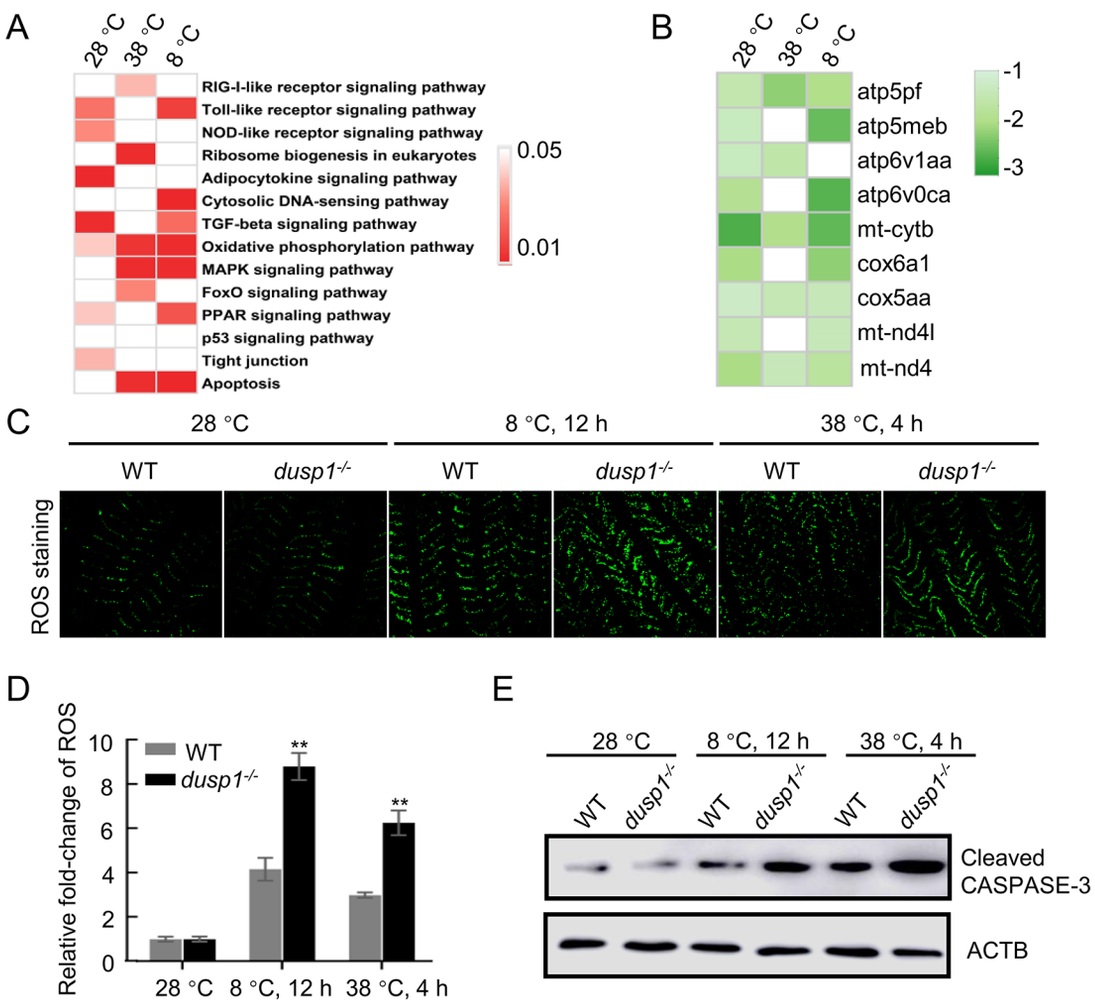

Figure 3 Disrupted MAPK and redox regulation and elevated susceptibility to thermal stress detected in gills of *dusp1*-deleted fish measured at three temperature-time points (28 °C, 38 °C 4 h, 8 °C 12 h)

A: KEGG enrichment analysis of DEGs between *dusp1*$^{-/-}$ and WT treated at different temperatures. B: Markedly reduced expression of mitochondrial-related genes in KEGG "oxidative phosphorylation" pathway identified in *dusp1*$^{-/-}$ versus WT zebrafish at three temperatures. Log_2 transformation of gene fold-change is indicated by the color-coded scale. C: DCFH-DA probe for ROS in the gills of *dusp1*$^{-/-}$ and WT zebrafish under different temperature treatments. Scale bar: 50 μm. D: Statistics of ROS fluorescence intensity detected in the gills of temperature-treated *dusp1*$^{-/-}$ and WT fish with ImageJ software. Statistically significant results between *dusp1*$^{-/-}$ and WT zebrafish are indicated by asterisks. Level of expression in WT (28 °C) was used as a normalizing factor and set to 1. Sample size: n=6 for each measurement, one-way ANOVA, **: P<0.01. E: Western blot assays of activated caspase-3, reflecting severity of mitochondrial-dependent apoptosis. ACTB was used as the loading control.

(Figure 3E). These results indicate cellular redox dysregulation in WT and especially *dusp1*$^{-/-}$ fish under adverse thermal conditions.

Impaired mitochondrial structure and function in *dusp1*$^{-/-}$ fish

To understand the cellular basis for the reduced ability of *dusp1*$^{-/-}$ fish to cope with adverse temperatures, we examined mitochondrial integrity. Based on light microscopy, we observed an increase in the number of mitochondria in the gills of *dusp1*$^{-/-}$ fish under all three conditions, with a greater increase in *dusp1*$^{-/-}$ fish under thermal stress relative to WT fish (Figure 4A, B). We then examined mitochondrial integrity based on scanning electron microscopy. Mitochondria in the *dusp1*$^{-/-}$ fish were irregularly shaped and exhibited marked membrane damage (Figure 4C). ATP production in the *dusp1*$^{-/-}$ fish gills was substantially reduced at all three temperatures (Figure 4D). Increased mitochondrial fragmentation in the *dusp1*$^{-/-}$ fish yielded no significant differences in oxygen consumption under normal temperature but resulted in significantly slower oxygen consumption under cold and hot exposure compared to the WT fish (Figure 4E). These results suggest that *dusp1* is crucial for maintaining mitochondrial structure and oxidative phosphorylation in zebrafish.

Signaling pathways of DUSP1 in maintaining mitochondrial integrity

As a protein phosphatase, DUSP1 regulates three key kinases of the MAPK pathway, i.e., P38, ERK1/2, and JNK. Here, we investigated the expression levels of these three kinases in

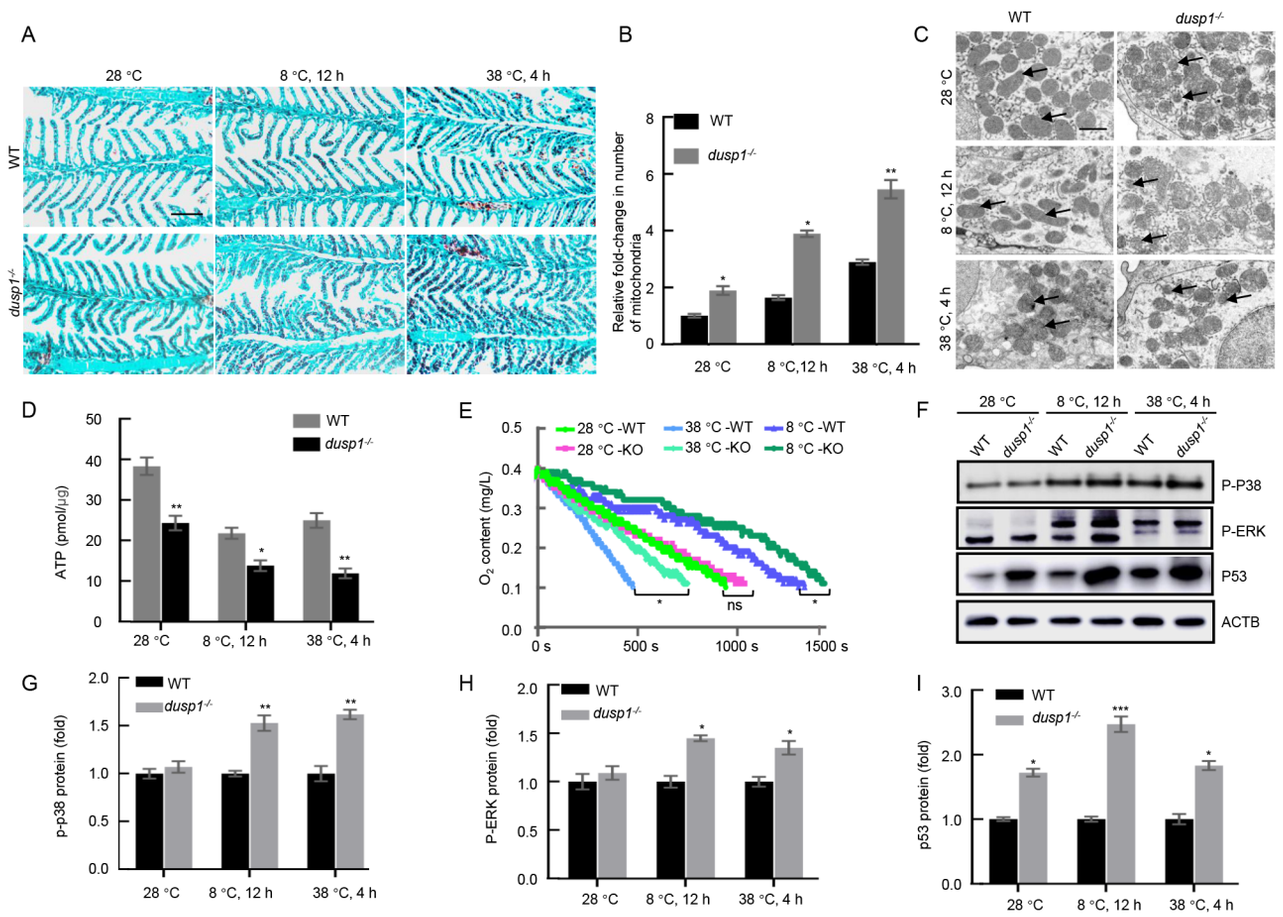

Figure 4 Dusp1 deficiency resulted in impaired mitochondrial structure and function

A: Scarlet (red) and brilliant green (blue) staining of gill sections of *dusp1*$^{-/-}$ and WT zebrafish under different temperature treatments. Mitochondria are in dark red and gill filaments are in green. Scale bar: 50 μm. Sample size=6 for each temperature-time treatment. B: Relative intensity of red fluorescence of the gill reflecting average number of mitochondria present in the gill section. Student's t test, *: P<0.05; **: P<0.01. Sample size: n=6. C: Transmission electron microscopy of mitochondrial structure in the gills of *dusp1*$^{-/-}$ and WT zebrafish under different temperature treatments. Dark circular structures are typical mitochondria. Mitochondria with abnormal shapes are indicated by arrows. Scale bar: 1 μm. D: ATP production measured by ATP Assay Kit (Beyotime, China) in *dusp1*$^{-/-}$ and WT zebrafish gills under different temperature treatments. Student's t test, *: P<0.05; **: P<0.01. Sample size: n=6 for each temperature-time point. E: Oxygen consumption rate measured using a respiratory oxygen consumption meter in *dusp1*$^{-/-}$ and WT fish under different temperature treatments. Sample size: n=6 for each curve, one-way ANOVA, *: P<0.05, ns: No significant difference. F–I: Western blot analyses of p-P38, p-ERK, and p53 in *dusp1*$^{-/-}$ and WT zebrafish exposed to different temperatures. Sample size n=6 for each measurement.

the gills of *dusp1*$^{-/-}$ fish and found that the phosphorylated forms of P38 and ERK1/2 were significantly elevated (Figure 4F–H), consistent with the loss of specific phosphatase activity of DUSP1 and indicating up-regulation of the MAPK/P38 and MAPK/ERK1/2 pathways. Elevation of these two pathways profoundly affects cell proliferation and death (Kolch, 2005; Koul et al., 2013; Lavoie & Therrien, 2015; Uhlitz et al., 2017). One of the key cell-fate determinants regulated by P38 is P53 (Obergasteiger et al., 2018; Perfettini et al., 2005). Indeed, in the *dusp1*$^{-/-}$ fish, P53 was markedly up-regulated in the gill cells, especially under adverse temperatures (Figure 4F, I). Increased P53 activates BAX, which promotes ROS production in the mitochondria (Liu et al., 2008a). However, it has also been reported that P53 regulates DUSP1 in response to oxidative damage (Liu et al., 2008b). Therefore, DUSP1 appears to play a key role in cell fate determination by regulating P53 when a cell faces lower and upper lethal temperatures.

Based on the widespread mitochondrial fragmentation in the *dusp1*$^{-/-}$ gill cells, another arm of DUSP1 in cell-fate regulation may be related to mitochondrial fission, as MAPKs such as p-P38 (Gui et al., 2020) and p-ERK1/2 (Kashatus et al., 2015; Pyakurel et al., 2015) are known regulators of mitochondrial integrity. However, the lack of specific antibodies against fish proteins hindered delineation of the players involved in this pathway. Thus, given the high conservation of the dusp1 and MAPK pathways, we used human HEK293T cells to study the molecular signaling pathways in more detail with available antibodies.

DUSP1-MAPK-DRP1 axis in regulating mitochondrial integrity and ROS production in human cells

DUSP1 is highly conserved between fish and mammals in terms of sequences (Supplementary Figure S4A) and cold- and high-temperature inducibilities (Supplementary Figure S4B). To further elucidate the factors involved in the signal transduction pathways in DUSP1-regulated thermal tolerance, we generated *DUSP1*-deficient HEK293T cells (Supplementary Figure S4C, D). *DUSP1* knockout resulted in increased ROS production (Figure 5A, B), higher apoptotic susceptibility (Figure 5C, D), slower cell proliferation (Figure 5E), higher caspase-3 cleavage (Figure 5F), increased mitochondrial fragmentation (Figure 5G, H), and significantly reduced mitochondrial membrane potential (Figure 5I, J) and ATP production (Figure 5K) under cold and heat stress. Overall, the *DUSP1* knockout HEK293T cells phenocopied what occurred in the *dusp1*$^{-/-}$ fish gills, suggesting that this cell line is suitable for delineating the factors that regulate mitochondrial integrity under thermal stress.

We examined the correlation between P38 and P53 in the human cell line under thermal stress. Consistent with the results in fish gills, the p-P38 and P53 protein levels were significantly increased in the *DUSP1*-KO cells under both cold and heat challenges (Figure 6A, C). The direct effect of P38 on P53 induction was demonstrated by the addition of the P38 inhibitor Y27632, which suppressed the increase in the P53 protein in the *DUSP1*-KO cells (Figure 6D, F) compared to when the P38 inhibitor was absent (Figure 6A). We then profiled the level of P53-dependent BAX protein (Selvakumaran et al., 1994), a trigger for apoptosis, and found it was increased under low and high temperature stress (Figure 6G, H), corresponding to the elevated apoptotic signals in the *DUSP1*-deficient cells.

Recent research has shown that p-DRP1Ser616, a phosphorylation product induced by MAPKs, plays an essential role in mitochondrial fission (Han et al., 2020). Thus, we next examined whether phosphorylation of S616 of DRP1 is responsible for the excessive mitochondrial fission under thermal stress. As expected, the levels of Ser616-phosphorylated DRP1 (p-DRP1Ser616) were significantly induced in the *DUSP1*-deficient cell line under both cold and heat stress (Figure 6I, J).

In conclusion, we illustrated a conserved vertebrate function of dusp1 in maintaining cellular homeostasis by regulating mitochondrial integrity under lethal temperatures (Figure 7). Briefly, lethal temperature stress up-regulated DUSP1, which dephosphorylated P38 and ERK1/2, resulting in reduced P53 and phosphorylated DRP1, respectively. Reduction of these two factors prevented mitochondrial-dependent apoptosis and ROS accumulation. However, lethal temperatures can directly increase cellular ROS production through MAPK-independent processes that promote MAPK activation (Son et al., 2013). Therefore, the DUSP1-MAPK-DRP1 axis may be one of the interconnected signaling pathways that regulate thermal tolerance in human cells and zebrafish.

DISCUSSION

Due to the complexity of thermal responses, the molecular mechanisms underpinning thermal tolerance limits of organisms are an important but unresolved question. In the current study, we first identified the gill as the organ most sensitive to thermal changes and identified DUSP1 as an important regulator of cellular thermal sensitivity in this organ. Notably, we found that knockout of *dusp1* reduced the thermal tolerance limit of zebrafish under both cold and heat challenges due to accelerated gill cell apoptosis. These findings suggest that the mechanisms underpinning cellular-level thermal susceptibility help set the thermal tolerance limits in ectothermal animals, and identifying cell types with the weakest tolerance may be key to deciphering the molecular mechanisms. In addition to zebrafish, the gills have also been identified as the most thermally sensitive organ in other species such as tilapia (Hu et al., 2016) and medaka (Hu et al., 2021) (Supplementary Figure S2). However, these observations do not exclude the possibility that other organs may be more vulnerable in other ectothermal species. For example, the heart is suspected to be the first organ to fail at the upper lethal temperature in salmonids (Farrell, 2002) and porcelain crabs (Somero, 2002). Alternatively, temperature-induced declines in neural function are suggested to constrain thermal tolerance limits in fish (Somero & DeVries, 1967). Thus, more comprehensive studies are warranted to generate a more complete thermal sensitivity atlas across different species of fish.

Temperature affects every aspect of cellular life from biosynthesis to metabolism, and cellular responses to thermal stress involve many stress response pathways, including the

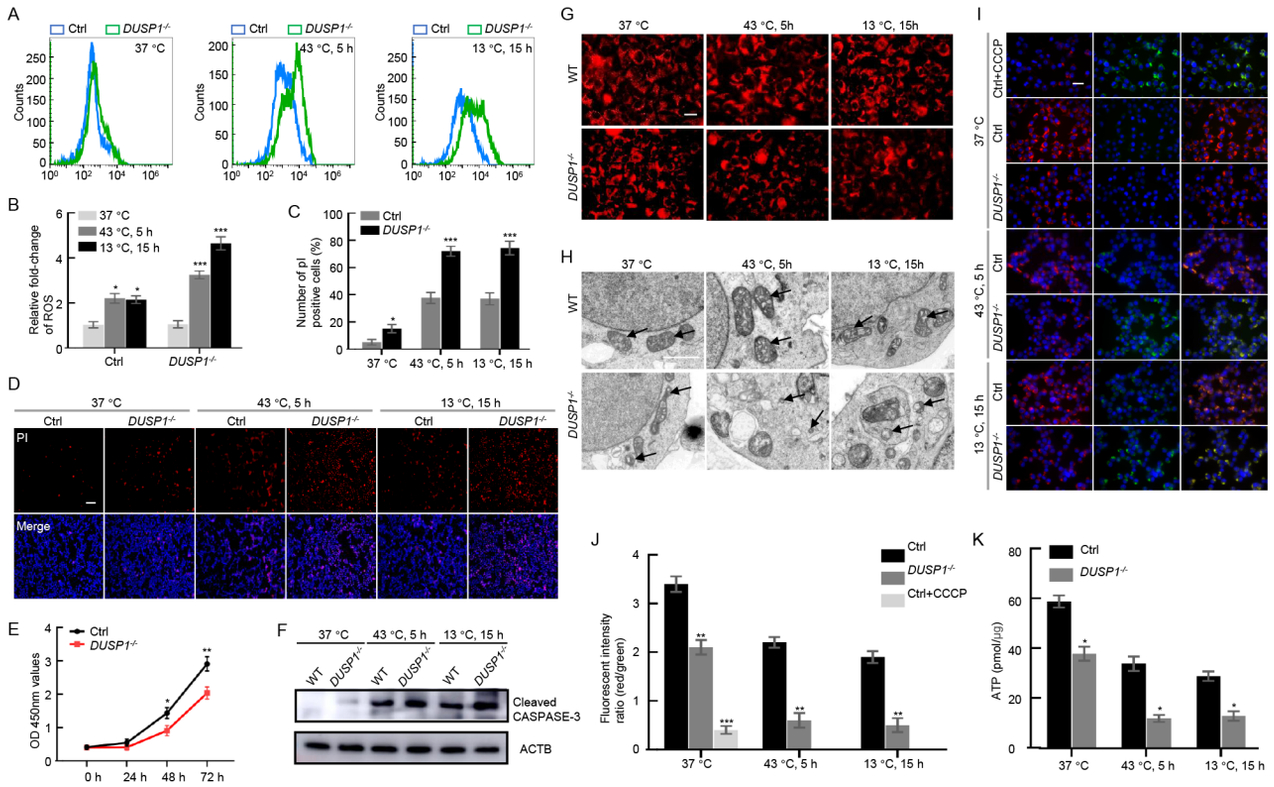

Figure 5 DUSP1 deletion caused redox dysregulation in human HEK293T cells

A: Flow cytometry measurement of ROS content at three temperature-time points (37 °C, 43 °C 5 h, 13 °C 15 h) using a ROS Assay Kit (Beyotime, China) in *DUSP1*$^{-/-}$ and control HEK293T cells. B: Statistics of ROS fluorescence intensity in samples measured in (A) analyzed using FlowJo software. One-way ANOVA, *: P<0.05; ***: P<0.001. C, D: PI staining to detect dead cells in *DUSP1*$^{-/-}$ and control HEK293T cells exposed to high and low temperatures. Scale bar: 100 μm. Student's t-test, *: P<0.05; ***: P<0.001. E: OD450 values of *DUSP1*$^{-/-}$ and control cells measured by CCK8 assay. One-way ANOVA, *: P<0.05; **: P<0.01. F: Western blot analysis of activated caspase-3 to detect mitochondrial dependent apoptosis in *DUSP1*$^{-/-}$ and control cells. ACTB was used as the loading control. G: MitoTracker staining of *DUSP1*$^{-/-}$ and control cells to reveal mitochondrial morphology at different temperatures. Scale bar: 20 μm. H: Transmission electron microscopy of mitochondrial structure in *DUSP1*$^{-/-}$ and WT HEK293T cells exposed to three temperatures. Arrows in panels of *DUSP1*$^{-/-}$ cells indicate fragmented mitochondria. Scale bar: 2 μm. I, J: JC-1 probe to measure mitochondrial membrane potential in *DUSP1*$^{-/-}$ and WT cells examined under fluorescence microscopy. CCCP was used as a positive control to induce a decrease in mitochondrial membrane potential. Scale bar: 20 μm. One-way ANOVA, **: P<0.01; ***: P<0.001. K: Relative levels of ATP production in *DUSP1*$^{-/-}$ and control cells exposed to three temperatures. One-way ANOVA, *: P<0.05.

unfolded protein response (Somero, 2020), transforming growth factor beta (TGF-β) (Mortzfeld et al., 2019), and MAPK signaling pathways (Sharma et al., 2005). Despite the complexity and diversity of these responses, excessive accumulation of ROS is a common feature in thermally stressed cells. Our results indicated that both upper and lower lethal temperature exposure resulted in excessive intracellular ROS accumulation in fish and human cells (Figures 3, 5). Excessive intracellular ROS is an important contributor to cell damage (Liochev, 2013) and may lead to cell death (Ryter et al., 2007). During cold stress, cells of the liver, muscle, and central nervous system of fish initiate protective responses to combat the increase in ROS production and susceptibility (Pörtner, 2010; Tseng et al., 2011). Studies of Antarctic fish living under persistent freezing regimes have found that up-regulation of the anti-ROS system is an important transcriptomic and genomic feature of these fish (Chen et al., 2008, 2019; Kim et al., 2019) to survive extremely cold temperatures. Therefore, restricting ROS production and mitigating ROS-induced cellular damage/death is fundamental for improving thermal tolerance in fish.

Mitochondria are a major source of ROS (Ott et al., 2007), and mitochondrial dysfunction can lead to aberrant ROS production (Murphy, 2009). The role of mitochondria in setting the thermal tolerance limit of ectotherms remains controversial (Chung and Schulte, 2020). *In vitro* measurements have suggested that mitochondria can function at temperatures much higher than those that limit organismal function (Pörtner, 2002; Somero, 2002), indicating a higher level of process in determining the whole-organismal thermal limits. However, a link between mitochondrial failure and failure of higher-level processes such as cardiac function has been suggested in numerous species (Iftikar & Hickey, 2013; Iftikar et al., 2014; Pörtner, 2001). Furthermore, in many species, patterns of mitochondrial genetic variation have been found to be correlated with environmental temperatures or temperature

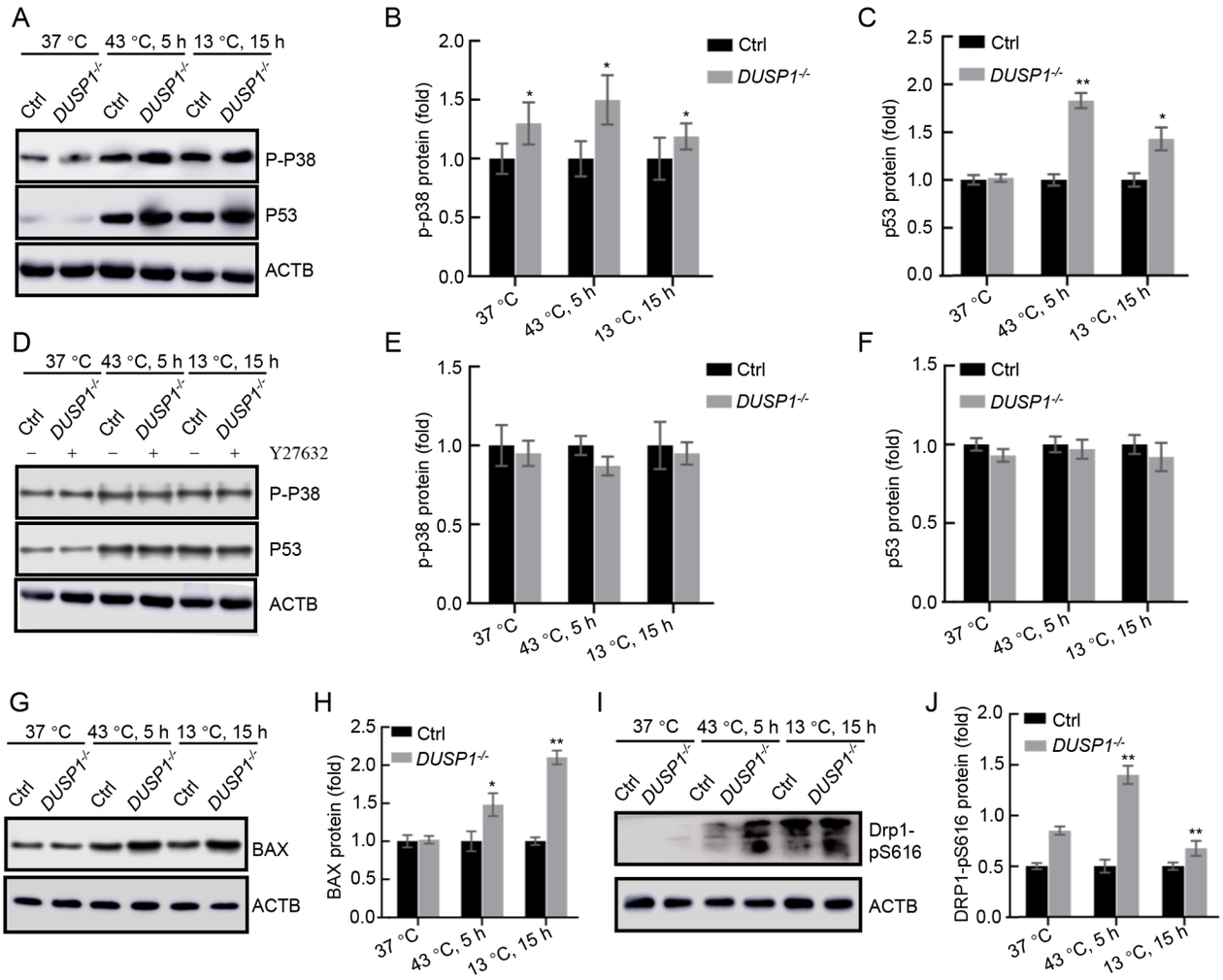

Figure 6 Western blot detection of major factors in DUSP1-MAPK-DRP1 axis in *DUSP1*$^{-/-}$ 293 T cells

A–C: Western blotting of p-P38 and P53 in *DUSP1*$^{-/-}$ and WT 293T cells at three temperature time points. D–F: Western blot analyses of p-P38 and p53 in presence of Y27632. G, H: Western blot analysis of apoptosis-related protein BAX. I, J: Western blotting showing increased phosphorylation of DRP1 at S616 in *DUSP1*$^{-/-}$ cells. ACTB was used as the loading control.

proxies where species inhabit (Ballard and Whitlock, 2004; Balloux et al., 2009; Cheviron and Brumfield, 2009; Consuegra et al., 2015; Dowling, 2014; Silva et al., 2014). These observations suggest that mitochondria may impose constraints on whole-organism thermal biology. In the current study, we revealed *in vivo* evidence that the structure and function of mitochondria were impaired under lethal cold and heat challenges, and that the degree of mitochondrial impairment that occurred in the most sensitive tissue (the gills) was linked to the lower and upper thermal tolerance limits of the whole organism. Notably, thermal stress induced excessive mitochondrial fragmentation and membrane leakage, resulting in lower ATP production and increased ROS accumulation, leading to cell death and whole-organism failure. Therefore, improving mitochondrial integrity and ROS scavenging is essential for cells and organisms to cope with acute temperature stress (Gerber et al., 2021; Iftikar & Hickey, 2013; Pörtner, 2010; Tseng et al., 2011).

In the current study, we delineated the pivotal function of DUSP1, an upstream regulator of the MAPK signaling pathway, in determining thermal adaptability in zebrafish gills and HEK cells. We found that DUSP1 dephosphorylated elevated p-P38 and p-ERK1/2 levels in cells under thermal stress, which attenuated overactive MAPK signaling and protected sensitive cells from excessive damage. DUSP1, MAPKs, P53, and ROS formed an interconnected signaling network as part of a more complicated cellular signaling network that regulates mitochondrial integrity and function and partially determines thermal tolerance limits in zebrafish. In this signaling network, MAPKs (i.e., P38 and ERK1/2), P53, and ROS are inter-promoting, forming a positive feedback loop, while DUSP1 is an important negative factor attenuating this feedback loop (Figure 7), which is essential for maintaining cellular ROS homeostasis to avoid excessive cell death. P53, which connects both MAPKs and ROS, acts as a threshold regulator of cellular homeostasis, determining the survival or death of stressed cells (Beyfuss & Hood, 2018; Wu, 2004). In this system, increased DUSP1 expression may be

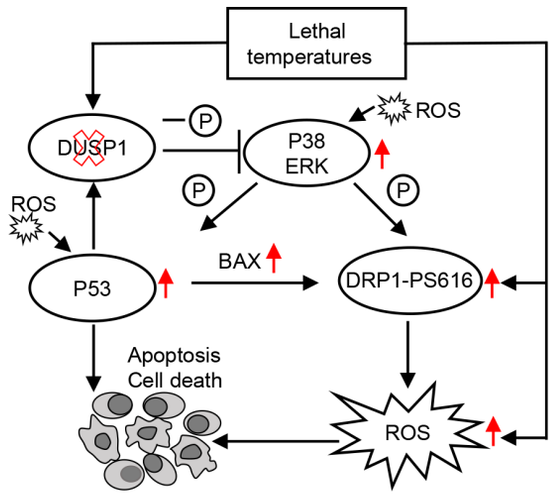

Figure 7 Proposed DUSP1-MAPK-DRP1 signaling cascade regulating thermal tolerance limit in zebrafish

Red arrows indicate elevation in proteins when *dusp1* is deleted (indicated by red cross).

beneficial for cell survival. Our preliminary data indicated that overexpression of *dusp1* in cells increased survival (Supplementary Figure S5), and the reintroduction of *dusp1* into *dusp1*$^{-/-}$ zebrafish embryos increased their survival under lethal temperature challenge. These results provide empirical evidence for the function of dusp1 in regulating the thermal tolerance limit in human cells and zebrafish.

MAPK signaling pathways exist widely in eukaryotes, including yeast, plants, and animals. They are important cell signaling modules that sense stimuli from upstream signaling molecules and propagate by a cascade of phosphorylation/dephosphorylation events (Jonak et al., 2002). In this way, the stress signal is amplified and transmitted to the target protein, causing a series of physiological and biochemical reactions in the cell to exert anti-stress functions (Ichimura et al., 2002). Our work and other studies suggest that overactivated MAPKs (p-P38 and p-ERK1/2) trigger mitochondrial fission by inducing the phosphorylation of DRP1 at S616. This DRP1 site is conserved in fish and humans (Supplementary Figure S6), which may contribute to the same phenotypes of mitochondrial fragmentation and dysfunction observed in *dusp1*-deficient zebrafish and human cells. As an evolutionarily conserved signaling pathway, MAPKs cross-talk with other signaling pathways, such as the TGF-β/BMP pathway (Guo & Wang, 2009) and PI3K/Akt pathway (Aksamitiene et al., 2012). Therefore, the DUSP1-MAPK-DRP1 axis identified in the current study to function in thermal tolerance limit regulation is only part of the network that regulates thermal tolerance limits in zebrafish and human cells. Certainly, species may differ in their specific modulations in network connectivity, making them different in their ability to tolerate heat. However, despite its complexity, one of the ultimate determinants is the ability to maintain cellular redox homeostasis, which includes processes fundamentally involved in the functional integrity of mitochondria.

We found that *dusp1*$^{-/-}$ zebrafish had significantly lower oxygen consumption rates and reduced thermal tolerance under cold and heat challenges (Figure 4E). These results suggested a link between aerobic metabolic capacity and lethal temperature limit, consistent with the OCLTT model prediction, which proposes a central role of aerobic metabolic capacity in setting thermal tolerance limits (Pörtner et al., 2017). However, the extent to which damaged gills impair oxygen uptake, and whether the reduced ability to transport oxygen has set a limit to thermal tolerance in the mutant fish remains unclear. Furthermore, the extent to which damaged gills affect systemic ion balance and how this relates to the ionoregulatory collapse model of thermal tolerance limits has not yet been determined. Thus, further studies are needed to investigate the critically impaired capacities of mutant fish to test the models involved.

Another interesting finding of this study was the common MAPK pathways elicited by cells in response to cold and heat challenges, indicating that both are stressors to cellular homeostasis. The common DUSP1-MAPK-DRP1 signaling pathway involved in both cold and heat challenges implies that manipulating *Dusp1* expression may extend the thermal tolerance range of zebrafish at both ends, a feature desirable for aquaculture species. In addition to *Dusp1*, dozens of *Dusp* genes are present in fish and humans, which function to dephosphorylate activated MAPKs (Lang & Raffi, 2019). Among them, *Dusp6* is known to regulate mitochondrial fission (Ma et al., 2020). Therefore, it would be interesting to further explore the functions of this gene family in terms of thermal tolerance regulation and to examine their behavior under cold and heat challenges. Elucidating the key factors that differentiate organisms in terms of thermal tolerance limits will provide insights into the evolutionary fate of ectotherms facing global climate change and facilitate the development of new agricultural varieties with enhanced thermal tolerance.

DATA AVAILABILITY

All Illumina RNA sequencing data from this project were deposited at NCBI under BioProjectID PRJNA602594, National Genomics Data Center (GSA: CRA008815), and Science Data Bank (DOI: 10.57760/sciencedb.06296).

SUPPLEMENTARY DATA

Supplementary data to this article can be found online.

COMPETING INTERESTS

The authors declare that they have no competing interests.

AUTHORS' CONTRIBUTIONS

Y.W. and L.B.C. designed the experiment, completed data analysis, and wrote the manuscript. H.M.W., L.H.H., J.M.W., J.H.Y., H.B.N., and X.P.H. performed the experiments. Y.Z. and P.H. helped with analyses and constructive discussion. All authors read and approved the final version of the manuscript.

ACKNOWLEDGMENTS

The authors would like to thank Ying Lu for technical assistance during the study.

REFERENCES

Aksamitiene E, Kiyatkin A, Kholodenko BN. 2012. Cross-talk between mitogenic Ras/MAPK and survival PI3K/Akt pathways: a fine balance. *Biochemical Society Transactions*, **40**(1): 139−146.

Ballard JWO, Whitlock MC. 2004. The incomplete natural history of mitochondria. *Molecular Ecology*, **13**(4): 729−744.

Balloux F, Handley LJL, Jombart T, Liu H, Manica A. 2009. Climate shaped the worldwide distribution of human mitochondrial DNA sequence variation. *Proceedings of the Royal Society B:Biological Sciences*, **276**(1672): 3447−3455.

Beyfuss K, Hood DA. 2018. A systematic review of p53 regulation of oxidative stress in skeletal muscle. *Redox Report*, **23**(1): 100−117.

Cai JH, Yeh TF, Wei HW, Liu IH. 2019. Temperature-induced embryonic diapause in blue-breasted quail (*Coturnix chinensis*) correlates with decreased mitochondrial-respiratory network and increased stress-response network. *Poultry Science*, **98**(7): 2977−2988.

Chen LB, Lu Y, Li WH, Ren YD, Yu MC, Jiang SW, et al. 2019. The genomic basis for colonizing the freezing Southern Ocean revealed by Antarctic toothfish and Patagonian robalo genomes. *GigaScience*, **8**(4): giz016.

Chen ZZ, Cheng CHC, Zhang JF, Cao LX, Chen L, Zhou LH, et al. 2008. Transcriptomic and genomic evolution under constant cold in Antarctic notothenioid fish. *Proceedings of the National Academy of Sciences of the United States of America*, **105**(35): 12944−12949.

Cheviron ZA, Brumfield RT. 2009. Migration-selection balance and local adaptation of mitochondrial haplotypes in rufous-collared sparrows (*Zonotrichia capensis*) along an elevational gradient. *Evolution*, **63**(6): 1593−1605.

Chung DJ, Schulte PM. 2020. Mitochondria and the thermal limits of ectotherms. *Journal of Experimental Biology*, **223**(20): jeb227801.

Comalada M, Lloberas J, Celada A. 2012. MKP-1: a critical phosphatase in the biology of macrophages controlling the switch between proliferation and activation. *European Journal of Immunology*, **42**(8): 1938−1948.

Consuegra S, John E, Verspoor E, de Leaniz CG. 2015. Patterns of natural selection acting on the mitochondrial genome of a locally adapted fish species. *Genetics Selection Evolution*, **47**(1): 58.

Dilorio PJ, Holsinger K, Schultz RJ, Hightower LE. 1996. Quantitative evidence that both Hsc70 and Hsp70 contribute to thermal adaptation in hybrids of the livebearing fishes *Poeciliopsis*. *Cell Stress & Chaperones*, **1**(2): 139–147.

Dowling DK. 2014. Evolutionary perspectives on the links between mitochondrial genotype and disease phenotype. *Biochimica et Biophysica Acta* (*BBA*)-*General Subjects*, **1840**(4): 1393–1403.

Fader SC, Yu ZM, Spotila JR. 1994. Seasonal variation in heat shock proteins (hsp 70) in stream fish under natural conditions. *Journal of Thermal Biology*, **19**(5): 335−341.

Farrell AP. 2002. Cardiorespiratory performance in salmonids during exercise at high temperature: insights into cardiovascular design limitations in fishes. *Comparative Biochemistry and Physiology Part A:Molecular & Integrative Physiology*, **132**(4): 797−810.

Gerber L, Clow KA, Gamperl AK. 2021. Acclimation to warm temperatures has important implications for mitochondrial function in Atlantic salmon (*Salmo salar*). *Journal of Experimental Biology*, **224**(2): jeb236257.

Gerlach GF, Turay L, Malik KT, Lida J, Scutt A, Goldspink G. 1990. Mechanisms of temperature acclimation in the carp: a molecular biology approach. *American Journal of Physiology:Regulatory, Integrative and Comparative Physiology*, **259**(2): R237−R244.

Gracey AY, Fraser EJ, Li WZ, Fang YX, Taylor RR, Rogers J, et al. 2004. Coping with cold: an integrative, multitissue analysis of the transcriptome of a poikilothermic vertebrate. *Proceedings of the National Academy of Sciences of the United States of America*, **101**(48): 16970−16975.

Gui C, Ren YX, Chen JL, Wu X, Mao KM, Li HH, et al. 2020. p38 MAPK-DRP1 signaling is involved in mitochondrial dysfunction and cell death in mutant A53T α-synuclein model of Parkinson's disease. *Toxicology and Applied Pharmacology*, **388**: 114874.

Guo X, Wang XF. 2009. Signaling cross-talk between TGF-β/BMP and other pathways. *Cell Research*, **19**(1): 71−88.

Halpern BS, Walbridge S, Selkoe KA, Kappel CV, Micheli F, D'agrosa C, et al. 2008. A global map of human impact on marine ecosystems. *Science*, **319**(5865): 948−952.

Han HL, Tan JQ, Wang RX, Wan HD, He YH, Yan XX, et al. 2020. PINK1 phosphorylates Drp1^{S616} to regulate mitophagy‐independent mitochondrial dynamics. *EMBO Reports*, **21**(8): e48686.

Hellmann JJ, Byers JE, Bierwagen BG, Dukes JS. 2008. Five potential consequences of climate change for invasive species. *Conservation Biology*, **22**(3): 534−543.

Hu LH, Wang Y, Wang HM, Chen LB. 2021. Effects of different temperature stress on gill apoptosis of medaka *Oryzias latipes*. *Journal of Dalian Ocean University*, **36**(6): 929–936. (in Chinese)

Hu P, Liu ML, Liu YM, Wang JF, Zhang D, Niu HB, et al. 2016. Transcriptome comparison reveals a genetic network regulating the lower temperature limit in fish. *Scientific Reports*, **6**: 28952.

Hu P, Liu ML, Zhang DM, Wang JF, Niu HB, Liu YM, et al. 2015. Global identification of the genetic networks and *cis*-regulatory elements of the cold response in zebrafish. *Nucleic Acids Research*, **43**(19): 9198−9213.

Ichimura K, Shinozaki K, Tena G, Sheen J, Henry Y, Champion A. et al. 2002. Mitogen-activated protein kinase cascades in plants: a new nomenclature. *Trends in Plant Science*, **7**(7): 301−308.

Iftikar FI, Hickey AJR. 2013. Do mitochondria limit hot fish hearts? Understanding the role of mitochondrial function with heat stress in *Notolabrus celidotus*. *PLoS One*, **8**(5): e64120.

Iftikar FI, MacDonald JR, Baker DW, Renshaw GMC, Hickey AJR. 2014. Could thermal sensitivity of mitochondria determine species distribution in a changing climate?. *Journal of Experimental Biology*, **217**(13): 2348−2357.

Johnston PV, Roots BI. 1964. Brain lipid fatty acids and temperature acclimation. *Comparative Biochemistry and Physiology*, **11**(3): 303−309.

Jonak C, Ökrész L, Bögre L, Hirt H. 2002. Complexity, cross talk and integration of plant MAP kinase signalling. *Current Opinion in Plant Biology*, **5**(5): 415−424.

Ju Z, Dunham R, Liu Z. 2002. Differential gene expression in the brain of channel catfish (*Ictalurus punctatus*) in response to cold acclimation. *Molecular Genetics and Genomics*, **268**(1): 87−95.

Kanehisa M, Goto S, Furumichi M, Tanabe M, Hirakawa M. 2010. KEGG for representation and analysis of molecular networks involving diseases and drugs. *Nucleic Acids Research*, **38**(S1): D355−D360.

Kashatus JA, Nascimento A, Myers LJ, Sher A, Byrne FL, Hoehn KL, et al. 2015. Erk2 phosphorylation of Drp1 promotes mitochondrial fission and MAPK-driven tumor growth. *Molecular Cell*, **57**(3): 537−551.

Kim BM, Amores A, Kang S, Ahn DH, Kim JH, Kim IC, et al. 2019. Antarctic blackfin icefish genome reveals adaptations to extreme environments. *Nature Ecology & Evolution*, **3**(3): 469−478.

Kim D, Langmead B, Salzberg SL. 2015. HISAT: a fast spliced aligner with

low memory requirements. *Nature Methods*, **12**(4): 357−360.
Kim HJ, Lee HJ, Kim H, Cho SW, Kim JS. 2009. Targeted genome editing in human cells with zinc finger nucleases constructed via modular assembly. *Genome Research*, **19**(7): 1279−1288.
Kolch W. 2005. Coordinating ERK/MAPK signalling through scaffolds and inhibitors. *Nature Reviews Molecular Cell Biology*, **6**(11): 827−837.
Koul HK, Pal M, Koul S. 2013. Role of p38 MAP kinase signal transduction in solid tumors. *Genes & Cancer*, **4**(9–10): 342–359.
Kültz D, Burg M. 1998. Evolution of osmotic stress signaling via MAP kinase cascades. *Journal of Experimental Biology*, **201**(22): 3015−3021.
Lang R, Raffi FAM. 2019. Dual-specificity phosphatases in immunity and infection: an update. *International Journal of Molecular Sciences*, **20**(11): 2710.
Lavoie H, Therrien M. 2015. Regulation of RAF protein kinases in ERK signalling. *Nature Reviews Molecular Cell Biology*, **16**(5): 281−298.
Li B, Yi P, Zhang B, Xu CJ, Liu QY, Pi ZJ, et al. 2011. Differences in endoplasmic reticulum stress signalling kinetics determine cell survival outcome through activation of MKP-1. *Cellular Signalling*, **23**(1): 35−45.
Liochev SI. 2013. Reactive oxygen species and the free radical theory of aging. *Free Radical Biology and Medicine*, **60**: 1−4.
Liu B, Chen YM, Clair DKS. 2008a. ROS and p53: a versatile partnership. *Free Radical Biology and Medicine*, **44**(8): 1529−1535.
Liu YX, Wang JL, Guo JF, Wu JJ, Lieberman HB, Yin YX. 2008b. *DUSP1* is controlled by p53 during the cellular response to oxidative stress. *Molecular Cancer Research*, **6**(4): 624−633.
Logan CA, Somero GN. 2011. Effects of thermal acclimation on transcriptional responses to acute heat stress in the eurythermal fish *Gillichthys mirabilis* (Cooper). *American Journal of Physiology:Regulatory, Integrative and Comparative Physiology*, **300**(6): R1373−R1383.
Ma RN, Ma LN, Weng WJ, Wang YP, Liu HQ, Guo RJ, et al. 2020. DUSP6 SUMOylation protects cells from oxidative damage via direct regulation of Drp1 dephosphorylation. *Science Advances*, **6**(13): eaaz0361.
MacMillan HA. 2019. Dissecting cause from consequence: a systematic approach to thermal limits. *Journal of Experimental Biology*, **222**(4): jeb191593.
Mortzfeld BM, Taubenheim J, Klimovich AV, Fraune S, Rosenstiel P, Bosch TCG. 2019. Temperature and insulin signaling regulate body size in *Hydra* by the Wnt and TGF-beta pathways. *Nature Communications*, **10**(1): 3257.
Murphy MP. 2009. How mitochondria produce reactive oxygen species?. *Biochemical Journal*, **417**(1): 1−13.
Niu HB, Hu P, Cheng PL, Chu X, Hu C L, Chen LB. 2017. The role of *dusp1* downregulation in apoptosis of zebrafish ZF4 cells under cold stress. *Journal of Fishery Sciences of China*, **24**(5): 995−1002. (in Chinese)
Obergasteiger J, Frapporti G, Pramstaller PP, Hicks AA, Volta M. 2018. A new hypothesis for Parkinson's disease pathogenesis: GTPase-p38 MAPK signaling and autophagy as convergence points of etiology and genomics. *Molecular Neurodegeneration*, **13**(1): 40.
Ott M, Gogvadze V, Orrenius S, Zhivotovsky B. 2007. Mitochondria, oxidative stress and cell death. *Apoptosis*, **12**(5): 913−922.
Overgaard J, MacMillan HA. 2017. The integrative physiology of insect chill tolerance. *Annual Review of Physiology*, **79**: 187−208.
Peck LS, Morley SA, Richard J, Clark MS. 2014. Acclimation and thermal tolerance in Antarctic marine ectotherms. *Journal of Experimental Biology*, **217**(1): 16−22.
Perfettini JL, Castedo M, Nardacci R, Ciccosanti F, Boya P, Roumier T, et al. 2005. Essential role of p53 phosphorylation by p38 MAPK in apoptosis induction by the HIV-1 envelope. *Journal of Experimental Medicine*, **201**(2): 279−289.
Pfaffl MW. 2001. A new mathematical model for relative quantification in real-time RT–PCR. *Nucleic Acids Research*, **29**(9): e45.
Pichaud N, Ekström A, Hellgren K, Sandblom E. 2017. Dynamic changes in cardiac mitochondrial metabolism during warm acclimation in rainbow trout. *Journal of Experimental Biology*, **220**(9): 1674−1683.
Pörtner H. 2001. Climate change and temperature-dependent biogeography: oxygen limitation of thermal tolerance in animals. *Naturwissenschaften*, **88**(4): 137−146.
Pörtner HO. 2002. Physiological basis of temperature-dependent biogeography: trade-offs in muscle design and performance in polar ectotherms. *Journal of Experimental Biology*, **205**(15): 2217−2230.
Pörtner HO. 2010. Oxygen- and capacity-limitation of thermal tolerance: a matrix for integrating climate-related stressor effects in marine ecosystems. *Journal of Experimental Biology*, **213**(6): 881−893.
Pörtner HO. 2012. Integrating climate-related stressor effects on marine organisms: unifying principles linking molecule to ecosystem-level changes. *Marine Ecology Progress Series*, **470**: 273−290.
Pörtner HO, Bock C, Mark FC. 2017. Oxygen-and capacity-limited thermal tolerance: bridging ecology and physiology. *Journal of Experimental Biology*, **220**(15): 2685−2696.
Pyakurel A, Savoia C, Hess D, Scorrano L. 2015. Extracellular regulated kinase phosphorylates mitofusin 1 to control mitochondrial morphology and apoptosis. *Molecular Cell*, **58**(2): 244−254.
Rauch N, Rukhlenko OS, Kolch W, Kholodenko BN. 2016. MAPK kinase signalling dynamics regulate cell fate decisions and drug resistance. *Current Opinion in Structural Biology*, **41**: 151−158.
Robinson MD, McCarthy DJ, Smyth GK. 2010. edgeR: a Bioconductor package for differential expression analysis of digital gene expression data. *Bioinformatics*, **26**(1): 139−140.
Ryter SW, Kim HP, Hoetzel A, Park JW, Nakahira K, Wang X, et al. 2007. Mechanisms of cell death in oxidative stress. *Antioxidants & Redox Signaling*, **9**(1): 49−89.
Selvakumaran M, Lin HK, Miyashita T, Wang HG, Krajewski S, Reed JC, et al. 1994. Immediate early up-regulation of bax expression by p53 but not TGF beta 1: a paradigm for distinct apoptotic pathways. *Oncogene*, **9**(6): 1791−1798.
Sha JC, Zhang HY, Zhao Y, Feng XJ, Hu XY, Wang CR, et al. 2019. Dexmedetomidine attenuates lipopolysaccharide-induced liver oxidative stress and cell apoptosis in rats by increasing GSK-3β/MKP-1/Nrf2 pathway activity via the α2 adrenergic receptor. *Toxicology and Applied Pharmacology*, **364**: 144−152.
Sharma P, Sharma N, Deswal R. 2005. The molecular biology of the low‐temperature response in plants. *BioEssays*, **27**(10): 1048−1059.
Silva G, Lima FP, Martel P, Castilho R. 2014. Thermal adaptation and clinal mitochondrial DNA variation of European anchovy. *Proceedings of the Royal Society B:Biological Sciences*, **281**(1792): 20141093.
Somero GN, DeVries AL. 1967. Temperature tolerance of some Antarctic fishes. *Science*, **156**(3772): 257−258.
Somero GN, Hochachka PW. 1971. Biochemical adaptation to the environment. *American Zoologist*, **11**(1): 159−167.
Somero GN. 2002. Thermal physiology and vertical zonation of intertidal animals: optima, limits, and costs of living. *Integrative and Comparative Biology*, **42**(4): 780−789.
Somero GN. 2010. The physiology of climate change: how potentials for

acclimatization and genetic adaptation will determine ‘winners’ and ‘losers’. *Journal of Experimental Biology*, **213**(6): 912−920.

Somero GN. 2011. Comparative physiology: a “crystal ball” for predicting consequences of global change. *American Journal of Physiology:Regulatory, Integrative and Comparative Physiology*, **301**(1): R1−R14.

Somero GN. 2020. The cellular stress response and temperature: function, regulation, and evolution. *Journal of Experimental Zoology Part A:Ecological and Integrative Physiology*, **333**(6): 379−397.

Son Y, Kim S, Chung HT, Pae HO. 2013. Reactive oxygen species in the activation of MAP kinases. *Methods in Enzymology*, **528**: 27−48.

Stillman JH. 2003. Acclimation capacity underlies susceptibility to climate change. *Science*, **301**(5629): 65.

St-Pierre J, Charest PM, Guderley H. 1998. Relative contribution of quantitative and qualitative changes in mitochondria to metabolic compensation during seasonal acclimatisation of rainbow trout *Oncorhynchus mykiss*. *Journal of Experimental Biology*, **201**(21): 2961–2970.

Tomalty KMH, Meek MH, Stephens MR, Rincón G, Fangue NA, May BP, et al. 2015. Transcriptional response to acute thermal exposure in juvenile Chinook salmon determined by RNAseq. *G3 Genes| Genomes| Genetics*, **5**(7): 1335−1349.

Trapnell C, Williams BA, Pertea G, Mortazavi A, Kwan G, van Baren MJ, et al. 2010. Transcript assembly and abundance estimation from RNA-Seq reveals thousands of new transcripts and switching among isoforms. *Nature Biotechnology*, **28**(5): 511−515.

Tseng YC, Chen RD, Lucassen M, Schmidt MM, Dringen R, Abele D, et al. 2011. Exploring uncoupling proteins and antioxidant mechanisms under acute cold exposure in brains of fish. *PLoS One*, **6**(3): e18180.

Uhlitz F, Sieber A, Wyler E, Fritsche-Guenther R, Meisig J, Landthaler M, et al. 2017. An immediate–late gene expression module decodes ERK signal duration. *Molecular Systems Biology*, **13**(5): 928.

Vitousek PM, Mooney HA, Lubchenco J, Melillo JM. 1997. Human domination of Earth's ecosystems. *Science*, **277**(5325): 494−499.

Wancket LM, Frazier WJ, Liu YS. 2012. Mitogen-activated protein kinase phosphatase (MKP)-1 in immunology, physiology, and disease. *Life Sciences*, **90**(7–8): 237–248.

Wang J, Vasaikar S, Shi Z, Greer M, Zhang B. 2017. WebGestalt 2017: a more comprehensive, powerful, flexible and interactive gene set enrichment analysis toolkit. *Nucleic Acids Research*, **45**(W1): W130−W137.

Winter-Vann AM, Johnson GL. 2007. Integrated activation of MAP3Ks balances cell fate in response to stress. *Journal of Cellular Biochemistry*, **102**(4): 848−858.

Wu GS. 2004. The functional interactions between the p53 and MAPK signaling pathways. *Cancer Biology & Therapy*, **3**(2): 156−161.

Zhang MP, Zhang Y, Scheuring CF, Wu CC, Dong JJ, Zhang HB. 2012. Preparation of megabase-sized DNA from a variety of organisms using the nuclei method for advanced genomics research. *Nature Protocols*, **7**(3): 467−478.

Zhuang XN, Ma J, Xu SS, Zhang M, Xu GZ, Sun ZC. 2021. All-trans retinoic acid attenuates blue light-induced apoptosis of retinal photoreceptors by upregulating MKP-1 expression. *Molecular Neurobiology*, **58**(8): 4157−4168.